Published by Avanti Publishers

Global Journal of Energy Technology Research Updates

ISSN (online): 2409-5818

Exploring the Efficacy of Crab Shell-based Biochar for Adsorptive Uptake of Bromocresol Purple Dye in a Textile Wastewater: Kinetics and Mechanistic Studies

Julius N. Ndive[1], Okechukwu D. Onukwuli[2], Ifeoma A. Obiora-okafo[2], Somtochukwu G. Nnabuife[3] and Boyu Kuang[3,*]

[1]*Department of Chemical Engineering, Chukwuemeka Odumegwu Ojukwu University, Uli Anambra State, Nigeria*

[2]*Department of Chemical Engineering, Nnamdi Azikiwe University, Awka, Nigeria*

[3]*Faculty of Engineering and Applied Sciences, Cranfield University, Cranfield, MK43 0AL, United Kingdom*

ARTICLE INFO

Article Type: Research Article

Academic Editor: Wei Wang

Keywords:
Biochar,
Adsorption,
Wastewater,
FTIR and kinetics.

Timeline:
Received: June 01, 2025
Accepted: September 18, 2025
Published: December 10, 2025

Citation: Ndive JN., Onukwuli OD, Obiora-okafo IA, Nnabuife SG, Kuang B. Exploring the efficacy of crab shell-based biochar for adsorptive uptake of bromocresol purple dye in a textile wastewater: Kinetics and mechanistic studies. Glob J Energ Technol Res Updat. 2025; 12: 61-75.

DOI: https://doi.org/10.15377/2409-5818.2025.12.5

ABSTRACT

High-quality adsorbent derived from Crab Shell Activated Biochar (Fe_2O_3@BC) was effectively synthesised from discarded crab shells (CS) for the adsorptive elimination of Bromocresol purple colour (BCP) from textile wastewater. The structure of crab shell biochar (CSB) and crab shell activated biochar (CSAB) was looked at using SEM, and the light properties of the samples made from CSAB were checked with FTIR. The characterisation results suggested that the extracted chitin exhibited substantial properties necessary for surface phenomenon-driven matrices. This study looked at how well crab shell activated biochar and crab shell biochar can remove Bromocresol Purple (BCP) dye from water, finding that CSAB works better than CSB. The adsorption tests were conducted at varying pH levels, varied adsorbent doses, temperatures, and contact durations in batch trials. The kinetic analysis demonstrates that the removal efficiency was optimal according to the pseudo-second. The Weber–Morris intraparticle-diffusion analysis identified three operative adsorption sites. This low-cost crabshell-activated biochar, characterised by its advanced pore structure, distinctive surface properties, and superior adsorption capabilities, has the potential to function as an effective adsorbent for dye removal in textile effluent.

*Corresponding Author
Email: neil.kuang@cranfield.ac.uk
Tel: +(44) 7481 421141

1. Introduction

Pollution by hazardous compounds has become a major concern for environmental protection organisations [1]. Organic and inorganic wastes from household and industrial activities increasingly burden treatment systems and costs, threatening human and aquatic health. Consequently, researchers are tasked with developing waste-management and treatment strategies that are efficient, economical and environmentally sustainable [2]. Concern for health and the environment is catalysing advances in materials- and process-based water treatment. Dye-bearing effluents from textile, paper, printing and leather operations remain a leading pollution source. The wastewater from textile industry represents the main source to dye pollution. A variety of dyes and their degradation products can pose risks to living organisms. Over 10,000 dye formulations are in commercial use [3-5], with global production exceeding seven hundred tonnes annually and applications spanning multiple industries. Around ten to fifteen percent dyes were lost in effluents [6]. Wastewater is generated from a mix of industrial, domestic, agricultural, or commercial activities, as well as surface runoff or stormwater, and sewer inflow or infiltration [7, 8].

The textile industry significantly contributes to the economy of our nation. Unregulated and untreated waste disposal from these businesses generates significant water pollution in urban and industrial regions. Chemical processing accounts for approximately 70% of pollution in the textile sector. Cotton mills are recognised for their substantial water use in processes like sizing, bleaching, mercerisation, dyeing, printing, finishing, and washing. The chemical processing of textiles results in the discharge of substantial amounts of wastewater containing numerous contaminants. Given that these water streams impact the aquatic ecosystem in several ways, including the depletion of dissolved oxygen levels and the deposition of suspended material under anaerobic conditions, they warrant special consideration. Cotton offers an environmentally sustainable material; nonetheless, over 50% is reactive dyes [9].

The textile effluent produced by textile factories adversely affects soil fertility and degrades water resources, including lakes, rivers, ponds, and groundwater, harming both flora and fauna. The effluents are intensely pigmented, include elevated salt contents, and demonstrate high biological oxygen demand (BOD) values [10]. These dyes are ecologically detrimental if released untreated [11-14]. The emergence of diverse colours resulting from effluents in various sectors presents a substantial challenge for textile processing facilities [15-17]. Nonetheless, predicting the volume of textile wastewater generated is challenging, as each sector produces varying quantities of effluent based on production scale, methodologies, techniques, technologies, and the chemicals employed. Several studies [18-20] frequently criticise the textile sector for its effluent production. The textile industry uses substantial quantities of water during many processes. The water contains a significant quantity of complicated and detrimental compounds, including organic, inorganic, and polymeric substances. The textile effluent comprises several kinds of colouring chemicals, including dyes. Dye-effluent-laden water is not only hazardous but also detrimental to ecology, as its dark colouration obstructs sunlight, resulting in significant ecological issues [21-23]. Industrial waste needs to be cleaned up because it contains many harmful substances, including dyes that create serious environmental problems. The textile industry generally uses around 100,000 commercially produced dyes. The annual usage of these dyes is roughly 10 million kilogrammes, with around 1 lakh kilogrammes of this dye discharged into aquatic systems as effluent each year [24]. Poorly biodegradable dye colourants are often released directly to aquatic waters; their synthetic origin, complex aromatic frameworks and high stability raise environmental concern [25].

Various adsorbents exist for wastewater treatment; however, natural adsorbents have garnered significant interest owing to their cost-effectiveness, efficiency, and capability to treat wastewater [26]. The colour removal is extensively explored using several physiochemical techniques, including coagulation, ultrafiltration, electrochemical adsorption, and photooxidation. The aforementioned procedures are related to increased costs, reduced efficiency, and the production of harmful byproducts [27, 28]. Thus, adsorption is a prevalent technique for the wastewater dyes removal [29, 30].

2. Methods

2.1. Material Collection

Dye effluent was taken at Amawbia's textile facility (Anambra, Nigeria). One kilogram of crab shell was bought in Onitsha (Anambra). All reagents—$FeCl_2{\cdot}4H_2O$, $FeCl_3{\cdot}6H_2O$, H_3PO_4, NH_4OH, NaOH, H_2SO_4 and HCl—were analytical grade; supplier: Parchem, New Rochelle, NY (USA).

2.2. Sample Pre-treatment and Storage

Dye effluent was clarified by filtration to exclude particulates liable to hinder adsorption, then retained in amber glass pending analysis. Crab shells were rinsed with deionised water to remove adhering impurities and oven-dried at 323 K for 8 h to constant mass. The desiccated shells were pulverised to approximately 70 µm, particle size confirmed with a particle-size distribution analyser (Model 117.08, Malvern Instruments, USA), and the resulting powder sealed in airtight containers.

2.3. Adsorbent Preparations

The crab shell biochar (BC) powder was mixed with 85% H_3PO_4 in a 1:3 ratio, continuously swirled at 350 rpm, and heated to 70°C for 2 hours. Crab shell powder, abundant in acid, was carbonised in a tube furnace within an argon environment. The sample was subjected to a heating rate of 5°C/min until carbonisation temperatures of 300, 400, 500, 600, 700, and 800°C were attained, followed by a 35-minute hold at those temperatures. Subsequently, the sample was allowed to return to ambient temperature. The acquired crab shell biochar (BC) was meticulously rinsed with distilled water until a neutral pH was achieved. Thereafter, it underwent dehydration in a furnace maintained at 90°C for a duration of 12 hours. The processed crab shell biochar was pulverised and sieved to achieve a particle size of less than 50 µm.

Fe_2O_3/crabshell biochar was synthesised via a co-precipitation route. A 5 g portion of crabshell biochar was introduced into 30 mL of $FeCl_3{\cdot}6H_2O$ solution at ambient temperature and stirred for 1 h. pH was stabilised by titration with NH_4OH to generate the Fe_2O_3/crabshell composite. After washing with deionised water to near-neutral pH (~7), the material was dried at 90 °C for 12 h (forced-air oven) and subsequently stored in airtight containers [30, 31].

2.4. Instrumental Characterization

Physicochemical characterisation employed FTIR (Thermo Nicolet Nexus 470/670/870) for functional-group profiling and SEM (ZEISS EVO MA 17; EDX/WDS) for assessment of surface topography, in accordance with ASTM E1421–99 and ASTM E2809. Colour intensity was quantified by UV–Vis spectrophotometry.

2.5. Adsorption Studies

Adsorption tests covered pH 4, 5, 7, 9 and 10; adsorbent dosages of 0.7, 1.0, 1.6, 2.2 and 2.5 g; temperatures of 305.5, 308.0, 313.0, 318.0 and 320.5 K; and contact times of 30, 60, 120, 180 and 210 min. Solution pH was adjusted with 0.5 M H_2SO_4 or 0.6 M NaOH and verified using a Hanna meter (H12002-02). Following adjustment, Fe_2O_3/crab-shell biochar was dosed into 50 mL of dye effluent and agitated at 180 rpm for the prescribed contact period. After each run, the suspension was centrifuged and the supernatant retained for residual dye analysis.

The experimental kinetic data employed for mechanistic modelling was obtained by investigating the effects of time (15 – 300 min) and pH (4, 5, 7, 9, 10) on the dye adsorption capacity (qt). The efficacy of removal and the capacity for adsorption were evaluated using Equations (1) and (2), respectively.

$$BCP\ removal\ eff.(\%) = \frac{C_0 - C_t}{C_0}\ (100) \tag{1}$$

$$q_t = \frac{C_0 - C_t}{m} V \tag{2}$$

In the batch mass-balance notation, concentrations are reported in mg L^{-1}. We denote by C_0 the dye concentration measured before contact with the sorbent, and by C_t the value determined after a contact time t. The liquid working volume processed in each run is V (L), while the dry dose of Fe_2O_3/crab-shell biochar added at the start is m (g). The specific uptake at time t, q_t (mg/g), follows the standard relation $q_t = (C_0 - C_t)\ V / m$. In practice, C_0 and C_t are obtained from UV–Vis calibration, V corresponds to the set batch volume (e.g. 50 mL = 0.050 L for calculations), and m is the weighed dry mass of the composite used in that run.

2.6. Mechanistic Modelling

Film diffusion, intraparticle diffusion and bulk-phase transport together govern molecular movement in adsorption systems. Under the agitation conditions employed, bulk resistance is typically fast and therefore neglected during kinetic fitting. Consequently, control of uptake commonly resides either within the particle-surrounding boundary layer (film diffusion) or through the sorbent's internal pores (intraparticle diffusion). The mechanistic models summarised in Table **1** are accordingly used to diagnose the controlling step for BCP adsorption on Fe_2O_3–crab-shell biochar, as given by Eqs. (3) and (4).

Table 1: Kinetic and diffusion model equations.

Mechanistic Model	Mathematical Expression	Eq.
Webber Morris	$q_t = k_{id}t^{1/2} + C_{id}$	(3)
Liquid film diffusion	$\ln(1-F) = -k_{fd}t, \quad \left(F = \frac{q_t}{q_e}\right)$	(4)

3. Results and Discussion

3.1. Instrumental Characterization of Raw Crabshell

Fig. (**1**) demonstrates that the FTIR spectrum of BC displays 16 distinct peaks in the range of 75–90 transmittances. Significant peaks in the BC spectrum were identified at 3324.8, 2903.6, 1628.8, 1722.0, 1513.3, 1428.8, 1032.5, 898.3, and 834.9 cm^{-1}. The peak at 3324 cm^{-1} indicates the amino group (N-H stretching) in chitin and also corresponds to O–H stretching (alcohols, phenols). A broad band in the region 3000-3500 cm^{-1} indicates the presence of O-H stretching vibrations, which can be associated with water and hydroxyl groups in the shell's components. A prominent band at 1032 cm^{-1} is consistent with aliphatic C–N stretching in BCP. An absorption at 2903 cm^{-1} corresponds to amine C–H stretching, while features at 1628 and 1513 cm^{-1} are characteristic of amide I (secondary-amide C=O stretch) and amide II (C–N stretch coupled with N–H bending), respectively. Phosphorus-containing moieties are evidenced by bands within 898–834 cm^{-1} (P–O stretch) and by a signal at 1428 cm^{-1} assignable to C–N bending in methyl-substituted groups.

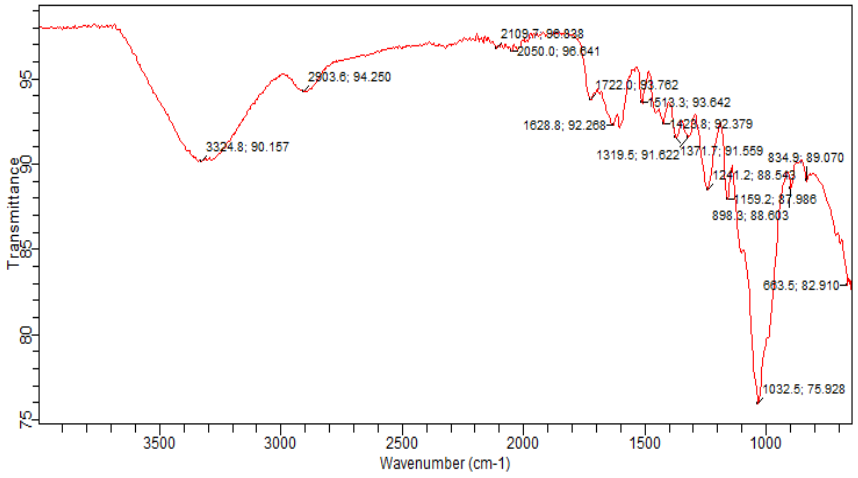

Figure 1: FTIR spectra of raw crabshell.

3.2. SEM Image Analysis

Fig. (**2**) shows the morphology of BC. The SEM micrograph reveals stronger surface cohesion, fewer discrete lamellar layers and an open, porous dark-field matrix, changes ascribed to the BC extraction process. This morphology favours particle adhesion in surface-dominated matrices, consistent with reports on crab-shell powder [32, 33].

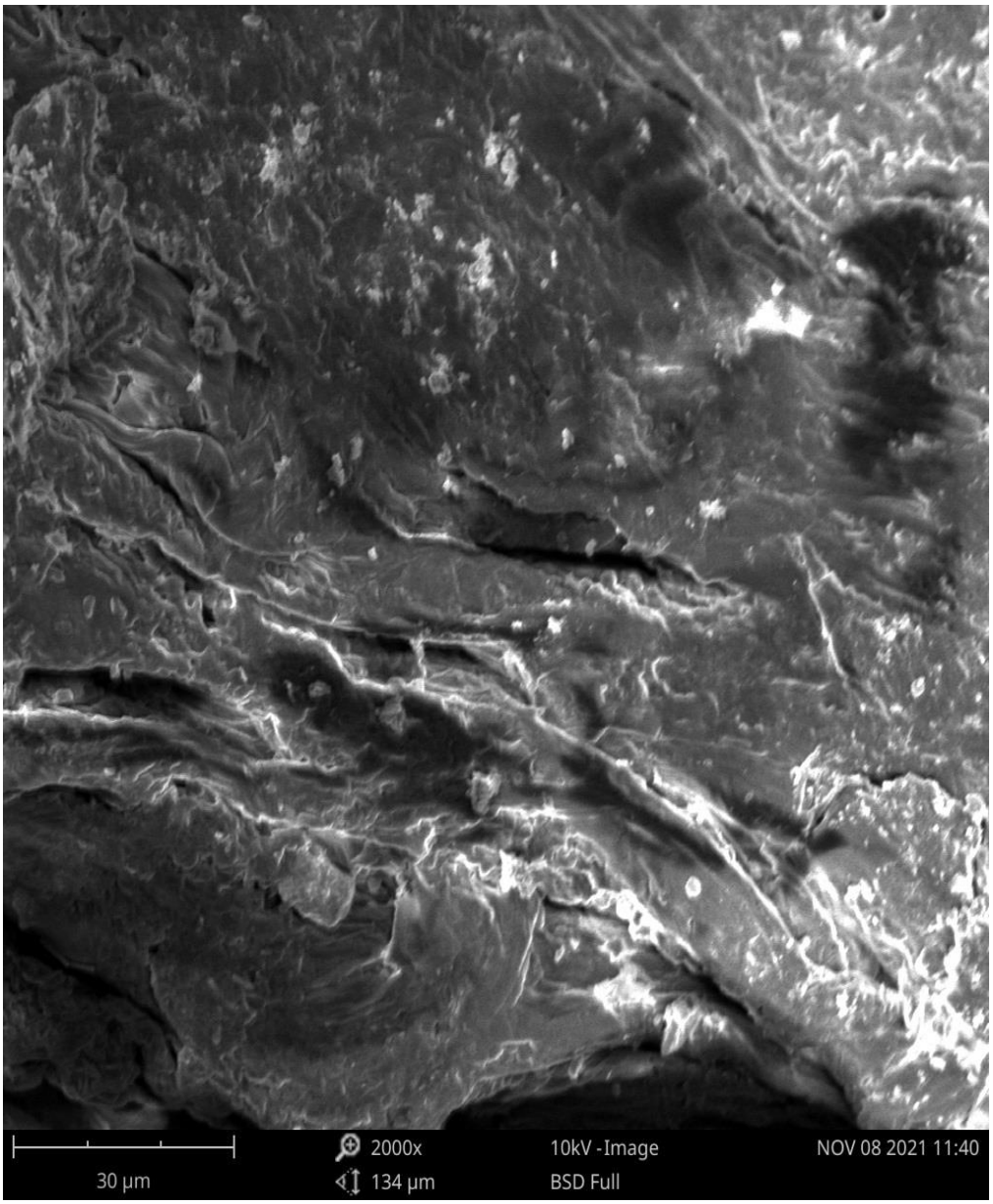

Figure 2: SEM micrograph of BC powder.

3.3. Process Factors Influence

The pH is a critical factor influencing the adsorption of dye molecules. The influence of the initial solution pH on the dye removal efficacy of bromocresol purple (BP) by activated (or inactive) crab shell biochar was assessed across a pH spectrum of 0 to 15. The studies were performed under the following parameters: carbonisation temperature of 700 °C, contact duration of 60 minutes, adsorbent dosage of 2.5 g/L, and ambient temperature of 25 °C. The dye's initial concentration was established at 50 mg/L. The dye clearance % is defined by Equation (5) [34].

$$\text{Removal rate } \% = \frac{c_0 - c_{(t)}}{c_0} \times 100 \quad (5)$$

where c_0 and c_t are the BP concentrations before adsorption and at time t, respectively.

As shown in Fig. (**3**), for the activated crab shell biochar (Fe_2O_3@BC), the dye removal efficiency was much higher in acidic pH conditions and began to decrease as the pH increased from 5 to 11. While at basic pH levels, the removal efficiency rapidly decreased. For the non-activated crab shell biochar (BC), the dye removal efficiency increased to 60% at acidic pH and slightly decreased as the pH increased from 3 to 11. From the graph, it was observed that the activated crab shell biochar exhibited higher removal efficiency in acidic dye solutions compared to the non-activated crab shell biochar.

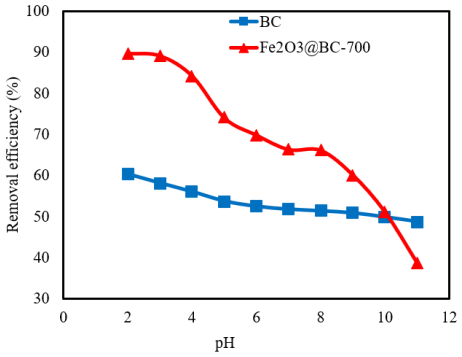

Figure 3: Effect of Ph vs. removal efficiency.

Since dye removal peaked at pH 1–2 (≈90%), the adsorption is most plausibly governed by Coulombic interactions between anionic dye species and protonated surface sites on the activated crab-shell biochar [35]. To optimise operating conditions, acidic media were therefore adopted, with pH 1–2 giving the highest efficiencies; pH 2 was selected for subsequent experiments.

3.4. Effect of Carbonization Temperature

The crab shells underwent initial acidification followed by carbonisation at different temperatures (200, 400, 600, and 800 °C) to generate activated crab shell biochar. Adsorption studies were conducted with the following parameters: contact duration of 60 minutes, pH of 7.0, adsorbent dosage of 2.5 g/L, and temperature of 25 °C. As shown in Fig. (**4**), BCP removal displays a clear dependence on carbonisation temperature. At low carbonisation temperatures, the crab shells were not completely carbonised, hindering the formation of the pore structure necessary for effective adsorption. The adsorption effect was significantly reduced. The results indicated that increasing the carbonisation temperature from 200 to 400 °C led to a progressive improvement in the adsorption efficiency of the crab shell biochar and the removal rate of the bromocresol purple dye solution. However, above 400 °C, the adsorption efficiency of the activated crab shell biochar began to decline slightly. At 500 °C, the adsorption efficiency declined to 40%. The highest dye removal efficiency was achieved at 800 °C.

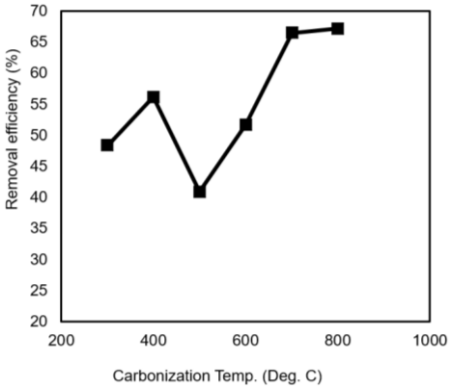

Figure 4: Plot of carbonization temp vs. removal efficiency.

3.5. Effect of Temperature

Batch adsorption tests used activated crab-shell biochar carbonised at 700 °C and operated at pH 2.0; the adsorbent dose was fixed at 2.5 g L^{-1}, with 50 mL aliquots of dye solution per run. Temperatures were set to 25–45 °C and time-courses recorded over 0–90 min, with 60 min taken as the nominal endpoint. Fig. (**5**) illustrates that at 25°C, the removal effectiveness surged from 0% to 70% rapidly, thereafter reaching a peak at approximately 40 minutes, after which adsorption decelerated. At 45°C, a more accelerated adsorption process was noted, with a removal efficiency of over 90% within 60 minutes (Fig. **5**). The results indicate that elevated temperatures improve dye removal effectiveness, with 45°C achieving the optimal adsorption performance. This is due to temperature-dependent alterations in the pore structure of the activated crabshell biochar, which affect its adsorption capability.

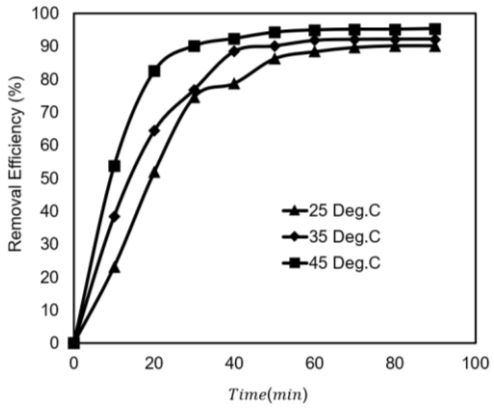

Figure 5: Plot of time vs. removal efficiency.

3.6. Time-Dependence of Adsorption

The effect of contact time on adsorption was tested for crab-shell biochar and Fe_2O_3@BC under controlled conditions (pH 2.0, 45 °C, 2.5 g L^{-1}) with prior carbonisation at 700 °C. The studies utilised a 50 mL dye solution with a contact period varying from 10 to 95 minutes. Fig. (**6**) presents the adsorption characteristics of crabshell biochar (BC) and activated crabshell biochar (Fe_2O_3@BC). The results for crabshell biochar (BC) indicated an initial quick rise in percentage adsorption from 0% to 55% within 10 to 20 minutes, followed by a plateau from 20 to 40 minutes, after which the adsorption effectiveness progressively diminished with increased contact time (Fig. **6**).

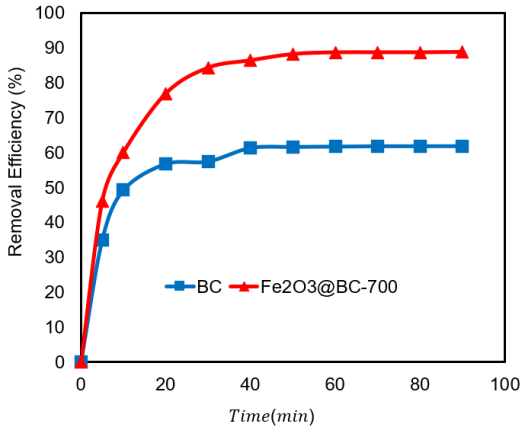

Figure 6: Effect of time vs. % dye adsorbed.

The adsorption effectiveness of bromocresol purple dye onto activated crabshell biochar (Fe_2O_3@BC) escalated swiftly from 0% to 75% in the initial 20 minutes, then decelerating between 20 and 95 minutes. This tendency is due to the increase in contact duration, which elevates the quantity of adsorbate caught while maintaining a constant adsorbent dosage. A larger quantity of active sites is initially accessible, promoting rapid adsorption. As

time advances, the remaining surface spots become increasingly difficult to occupy due to the repulsion between dye molecules and the bulk phase (Fig. **6**).

3.7. Effect of Dosage

Dye removal (%) was examined as a function of crab-shell adsorbent dosage (1–4 g/L) at 180 rpm using 50 mL dye solution. The experiments were conducted under defined parameters: a carbonisation temperature of 700°C, a pH of 2.0, a contact duration of 70 minutes, and a temperature of 45°C. Fig. (**7**) illustrates the relationship between adsorption efficiency and the increasing dosage of the adsorbent. Fig. (**7**) demonstrates that an increase in adsorbent dosage is associated with a higher percentage of dye adsorption. The activated crab shell biochar exhibited enhanced adsorption efficiency compared to the non-activated version. The activated crab shell biochar adsorbed nearly 90% of the dye, while the non-activated crab shell biochar attained approximately 60% adsorption.

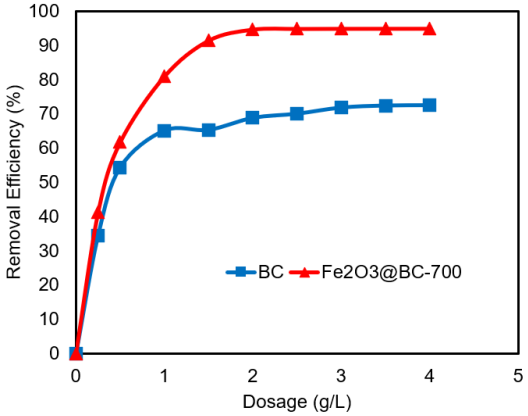

Figure 7: Effect of dosage vs. removal efficiency.

The findings demonstrate that an increase in adsorbent dosage is associated with a greater number of available sorption sites for adsorption (Fig. **7**). Greater dye removal stems from larger accessible surface area together with a higher number of adsorption sites at higher doses. Activated crab shell biochar exhibits a more advanced pore structure, leading to enhanced adsorption sites and a greater surface area compared to non-activated crab shell biochar.

3.8. Kinetic Study

Adsorption kinetics describe solute uptake over time and are central to assessing process efficiency [36]. To interpret the mechanism and identify the rate-limiting step (e.g. mass transfer or a surface reaction), we fitted three models: pseudo-first-order (PFO), pseudo-second-order (PSO) and the Elovich model [37]. Equations. (6)–(8) provide the corresponding rate expressions used in the analysis.

$$\ln(q_e - q_t) = \ln(q_e) - k_1 t \quad (6)$$

$$\frac{t}{q_t} = \frac{1}{K_2 q_e^2} + \frac{t}{q_e} \quad (7)$$

$$q_t = \left(\frac{1}{\beta}\right) \ln(\alpha\beta) + \left(\frac{1}{\beta}\right) ln\, t \quad (8)$$

Here, q_e and q_t (mg/g) denote the dye uptake at equilibrium and at time t, respectively. The PFO and PSO rate coefficients are k1 and K2, respectively. Regress $\ln(q_e - q_t)$ on t; the slope gives k_1 and the intercept gives $\ln q_e$. Regress t/q_t on t; the slope yields the PSO coefficient and the intercept equals the reciprocal of the equilibrium uptake.

Two kinetic models were applied to evaluate sample behaviour. Fig. (**8** and **9**) show that the adsorption of crab-shell activated biochar (CSAB) is described more accurately by the PSO model (R2 > 0.99) than by the PFO model

(R2 = 0.96); the same pattern is observed for CSB. The calculated q_e values (CSB: 63.694 mg/g, CSAB: 92.592 mg/g) closely aligned with the experimental q_e values (CSB: 61.90 mg/g, CSAB: 88.75 mg/g), as shown in the Appendix Table, suggesting that the pseudo-second-order model more accurately represents the actual adsorption process. Kinetic evidence points to chemisorption, with valence interactions arising from interfacial electron transfer [38, 39]. Among the tested models, the pseudo-second-order (PSO) fit yielded the highest coefficient of determination ($R^2 > 0.99$; Table **1**), outperforming the pseudo-first-order (PFO) and Elovich descriptions; the ranking PSO > PFO > Elovich is shown in Fig. (**10**). Accordingly, PSO best captures the rate behaviour for dye uptake on CSAB. The PFO rate expression is given in Equation (9).

$$log(q_e - q_t) = \log q_e - \frac{k_f}{2.303} t \quad (9)$$

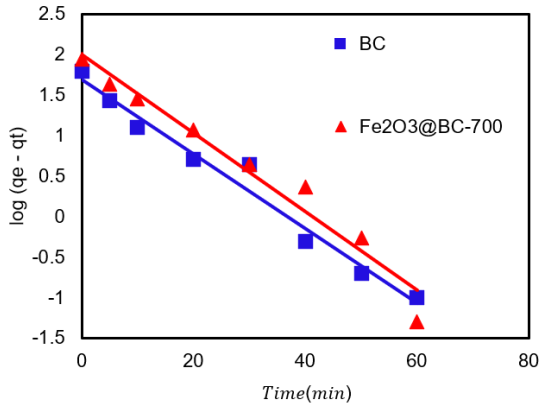

Figure 8: Plot of pseudo first order model.

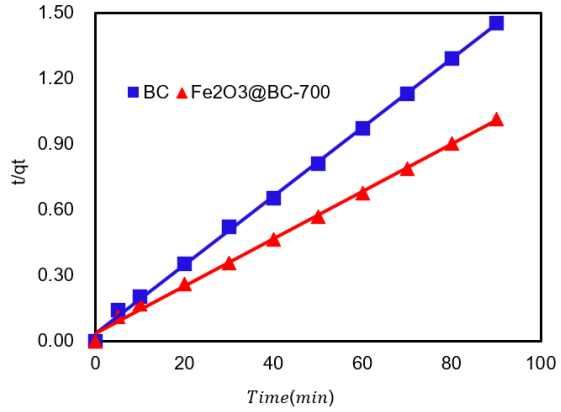

Figure 9: Plot of pseudo second order model.

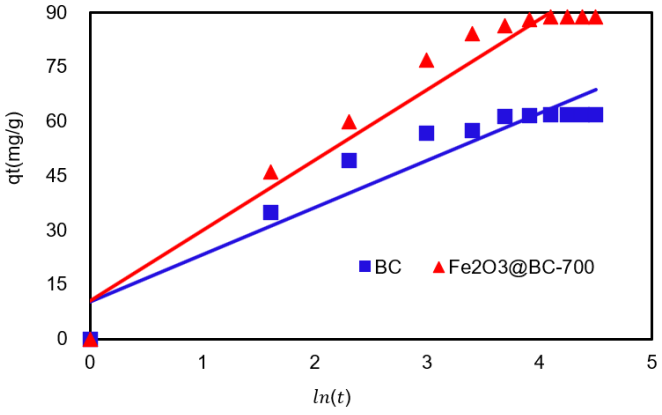

Figure 10: Plot of Elovich model.

3.9. Mechanistic Modelling

3.9.1. Weber–Morris intraparticle Diffusion Model

Stage-wise diffusion contributions to mass transfer during dye adsorption were evaluated using the Weber–Morris relation given in Equation (10).

$$q_t = k_{ipd} t^{1/2} + q_{ipd} \quad (10)$$

The Weber–Morris plot (qt vs. t1/2) is illustrated in Fig. (**11**), and the derived mechanistic parameters are detailed in the Appendix Table. The findings demonstrated that three separate regions participated in the sorption mechanism of the CSAB and CSB. The initial linear phase of film diffusion occurred during the sorption interval of 0 to 16 minutes. In the first 0–16 min, boundary-layer transport to outer surface sites prevailed on both CSAB and CSB; between 17 and 42 min, diffusion within particles became the main step. The second stage entailed the distribution of dye ions throughout the macropores, mesopores, and micropores of CSAB and CSB active sites. The third stage, occurring between 43 and 95 minutes, represents the equilibrium phase. CSAB displayed a higher qipd than CSB, consistent with greater boundary-layer resistance in CSAB. The high BCP concentration supplied the driving force for external mass transfer [40-42]. Non-zero intercepts in Fig. (**11**) indicate that both film and intraparticle diffusion operated.

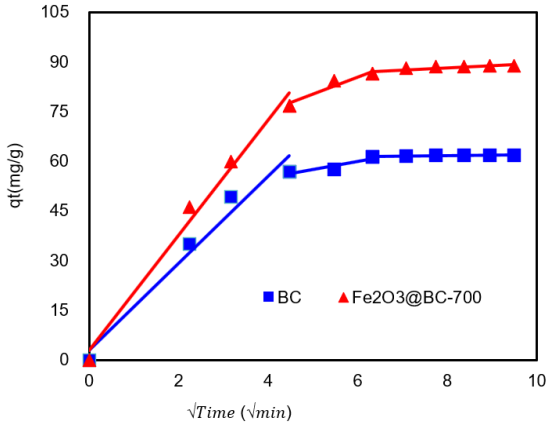

Figure 11: Plot of Webber-Morris intraparticle diffusion.

3.9.2. Liquid Film Diffusion Model (LFDM)

Fig. (**12**) shows ln(1-F) versus time, with parameter estimates listed in the Appendix Table. The fits are close to linear (R^2 = 0.99 for CSB and 0.95 for CSAB), but the deviation from perfect linearity indicates that pore diffusion is not the controlling step. Both R^2 and K_{fd} are higher for CSB, supporting film diffusion as the likely rate-governing step. The liquid-film diffusion relation is given in Equation (11).

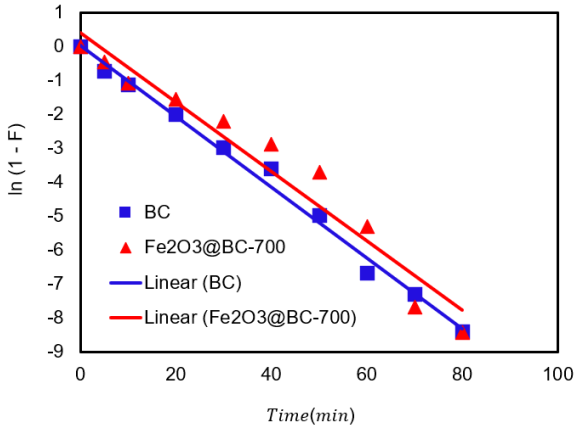

Figure 12: plot of liquid film diffusion model.

$$\ln(1-F) = -k_{fd}t, \left(F = \frac{q_t}{q_e}\right) \quad (11)$$

3.10. Homogenous Solid Diffusion Model (HSMD)

This represents an intraparticle diffusion model that elucidates the impact of mass transfer within an amorphous and homogeneous sphere [42-48]. Fig. (**13**) and the Table Appendix present the homogeneous solid diffusion model (HSMD) plot and associated model parameters. Fig. (**13**) presents the diffusion characteristics of CSB and CSAB. The recorded small Ds values for CSB (0.1467) and CSAB (0.1635) indicate that the adsorption rate diminishes as the adsorbent particle size increases, and conversely. This indicates that CSAB exhibits a larger particle size and enhanced adsorption efficiency relative to CSB, a conclusion further corroborated by the trend illustrated in Fig. (**13**). Equation (12) delineates the homogeneous solid diffusion model, which quantitatively characterises the observed adsorption behaviour.

$$\mathrm{F} = 6\left(\frac{D_s}{R^2\pi}\right)^{1/2} t^{1/2}, \left(F = \frac{q_t}{q_e}\right) \quad (12)$$

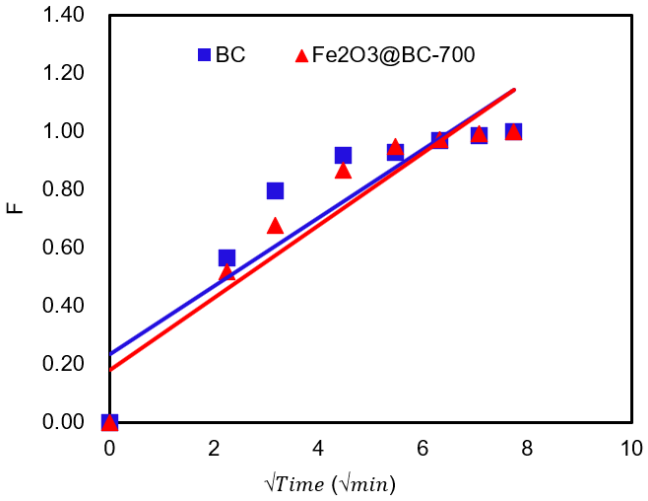

Figure 13: Plot of homogenous solid diffusion model.

4. Conclusions

This study developed and characterised crab-shell biochar (CSB) and activated crab-shell biochar (CSAB, Fe_2O_3@BC) for bromocresol purple (BCP) removal, using SEM/FTIR, batch adsorption tests across pH, dose, temperature and contact time, and kinetic–diffusion modelling (PFO, PSO, Elovich; Weber–Morris; liquid-film and homogeneous solid diffusion). Under optimised conditions (2.5 g L^{-1}, pH 2.0, 45 °C), CSAB consistently outperformed CSB and raw shell. Kinetic fits ranked PSO > PFO > Elovich (R^2 up to >0.99), and diffusion analysis indicated boundary-layer control with multi-stage intraparticle transport. Contributions include valorising waste crab shells into an efficient dye adsorbent and providing mechanistic evidence that clarifies the rate-governing step under acidic conditions. Limitations are the single-dye system, bench-scale batch tests, acidic operating window, and the absence of regeneration, leaching and competition assessments; these constrain immediate generalisation to complex effluents.

Future studies should test real textile wastewaters containing mixed dyes, salts and surfactants at practical pH, quantify reusability and stability via regeneration cycles and leaching checks, and extend to continuous-flow or column configurations with techno-economic and life-cycle analyses [36, 37, 49]. Optimising carbonisation/activation protocols to widen the effective pH range and reduce dose, and benchmarking CSAB against standard adsorbents under identical conditions, will further substantiate its applicability at scale.

Abbreviations

α (alpha)	=	Initial adsorption rate in Elovich model ($mg/g \cdot min$)
β (beta)	=	Desorption constant in Elovich model (g/mg)
BC	=	Biochar
BCP	=	Bromocresol Purple
C_0	=	Initial dye concentration (mg/L)
C_t	=	Dye concentration at time t (mg/L)
CS	=	Crab Shell
CSAB	=	Crab Shell Activated Biochar (also noted as Fe_2O_3@BC)
CSB	=	Crab Shell Biochar
D_s	=	Solid phase diffusion coefficient (m^2/s)
Eq.	=	Equation
FTIR	=	Fourier Transform Infrared Spectroscopy
HSMD	=	Homogeneous Solid Diffusion Model
LFDM	=	Liquid Film Diffusion Model
m	=	Mass of adsorbent (g)
PFO	=	Pseudo-First-Order kinetic model
PSO	=	Pseudo-Second-Order kinetic model
q_e	=	Equilibrium adsorption capacity (mg/g)
q_t	=	Adsorption capacity at time t (mg/g)
q_{ipd}	=	Intercept in Weber–Morris model (mg/g)
R^2	=	Coefficient of determination
Rpm	=	Revolutions per minute
SEM	=	Scanning Electron Microscopy
t	=	Time (min)
T	=	Temperature (°C or K depending on context)
UV	=	Ultraviolet
V	=	Volume of dye solution (L)
Fe_2O_3@BC	=	Iron oxide-loaded crab shell biochar (same as CSAB)
k_1	=	Rate constant for pseudo-first-order model ($1/min$)
k_2	=	Rate constant for pseudo-second-order model ($g/mg \cdot min$)
k_{fd}	=	Rate constant in liquid film diffusion model ($1/min$)
k_{ipd}	=	Intraparticle diffusion rate constant (mg/g·min^0.5)
Δ	=	Delta, used in difference expressions (if applied in formulas or contextually)

Conflict of Interest

The authors declare no competing interests.

Funding

The authors received no specific funding for this work.

Acknowledgements

The authors wish to acknowledge and thank the following organizations for their assistance toward the completion of this work: Chemical Engineering Department, Chukwuemeka Odumegwu Ojukwu University, Uli Anambra State Nigeria, Chemical Engineering Department, Nnamdi Azikiwe University Awka, Nigeria; Central Leather Research Institute, Chennai, India; India Institute of Chemical Technology, India; India National Science Academy/Centre for International Cooperation in Science, India; and Water Resources Center, Texas Tech University, Lubbock, TX, USA.

Authors' contributions

JNN was instrumental in the conception and design of the study, conducted the experiments, and authored the report. OD oversaw the research, aided with data analysis, and offered essential amendments to the report. IAO was involved in data acquisition, analysis, and manuscript editing. SGN facilitated material characterisation and supported experimental methodologies. BK performed proofreading and significantly altered the article for clarity and intellectual substance. All writers reviewed and endorsed the final manuscript and accept personal responsibility for their contributions. They have ensured that all issues about the accuracy or integrity of the work have been thoroughly explored and addressed.

References

[1] Menkiti M, Okoani O, Ejimofor M. Adsorptive study of coagulation treatment of paint wastewater using novel Brachystegiaeurycoma extract. 2018. https://doi.org/10.1007/s13201-018-0836-1

[2] Gupta VK, Atar N, Yola ML, Ustundag Z, Uzun L. A novel magnetic Fe@Au core-shell nanoparticles anchored graphene oxide recyclable nanocatalyst for the reduction of nitrophenol compounds. Water Res. 2014; 48: 210-17. https://doi.org/10.1016/j.watres.2013.09.027

[3] Banat IM, Nigam P, Singh D, Marchant R. Microbial decolorization of textile-dye-containing effluents: a review. Bioresour Technol. 1996; 58: 217-27. https://doi.org/10.1016/S0960-8524(96)00113-7

[4] Spadaro JT, Isabelle L, Renganathan V. Hydroxyl radical mediated degradation of azo dyes: evidence for benzene generation. Environ Sci Technol. 1994; 28(7): 123-30. https://doi.org/10.1021/es00056a031

[5] Robinson T, McMullan G, Marchant R, Nigam P. Remediation of dyes in textile effluent: a critical review on current treatment technologies with a proposed alternative. Bioresour Technol. 2001; 77(3): 247-55. https://doi.org/10.1016/S0960-8524(00)00080-8

[6] Forgacs E, Cserháti T, Oros G. Removal of synthetic dyes from wastewaters: a review. Environ Int. 2004; 30(7): 953-71. https://doi.org/10.1016/j.envint.2004.02.001

[7] Babu BR, Parande AK, Basha CA. Electrical and electronic waste: a global environmental problem. J Sustain Circular Econ. 2007; 25(4): 307-18. https://doi.org/10.1177/0734242X07076941

[8] Awomeso AJ, Taiwo AM, Gbadebo AM, Adenowo JA. Studies on the pollution of waterbody by textile effluents in Lagos, Nigeria. J Appl Sci Environ Sanit. 2010; 5(4): 353-9.

[9] Ohale PE, Chukwudi K, Ndive JN, Michael ME, Abonyi MN, Chukwu MM, *et al*. Optimization of Fe2O3@BC-KC composite preparation for adsorption of Alizarin red S dye: characterization, kinetics, equilibrium, and thermodynamic studies. R Surfaces Interfaces. 2023; 100157. https://doi.org/10.1016/j.rsurfi.2023.100157

[10] Stephenie A, Obiora-okafo E, Nnamdi NJ. Determination of local seeds (Melon and Fluted Pumpkin seeds): drying kinetics models. J Multidiscip Eng Sci Technol. 2021; 8(4): 13819-26.

[11] Deans JR, Dixon BG. Uptake of Pb2+ and Cu2+ by novel biopolymers. Water Res. 1992; 26(4): 469-72. https://doi.org/10.1016/0043-1354(92)90047-8

[12] Vilaseca M, Gutiérrez MC, López-Grimau V, López-Mesas M, Crespi M. Biological treatment of a textile effluent after electrochemical oxidation of reactive dyes. Water Environ Res. 2010; 82(2): 176-82. https://doi.org/10.2175/106143009X447902

[13] Kim Y, Kim C, Choi I, Rengaraj S, Yi J. Arsenic removal using mesoporous alumina prepared via a templating method. Environ Sci Technol. 2004; 38(3): 924-31. https://doi.org/10.1021/es0346431

[14] Muzzarelli RAA, Rocchetti R. Determination of the degree of acetylation of chitosans by first derivative ultraviolet spectrophotometry. Carbohydr Polym. 1985; 5(6): 461-72. https://doi.org/10.1016/0144-8617(85)90005-0

[15] Nigam P, Armour G, Banat IM, Singh D. Physical removal of textile dyes from effluents and solid-state fermentation of dye-adsorbed agricultural residues. Bioresour Technol. 2000; 72(3): 219-26. https://doi.org/10.1016/S0960-8524(99)00123-6

[16] Reddy CSK, Ghai R, Kalia VC. Polyhydroxyalkanoates: an overview. Bioresour Technol. 2003; 87(2): 137-46. https://doi.org/10.1016/S0960-8524(02)00212-2

[17] Ndive JN, Eze SO, Nnabuife SG, Kuang B, Rana ZA. Dual-chamber microbial fuel cell for azo-dye degradation and electricity generation in textile wastewater treatment. Waste Manag Bull. 2025; 3: 100195. https://doi.org/10.1016/j.wmb.2025.100195

[18] Porkodi K, Senthilkumaar S, Kalaamani P. Adsorption of dissolved reactive red dye from aqueous phase onto activated carbon prepared from agricultural waste. Bioresour Technol. 2006; 97(14): 1618-25. https://doi.org/10.1016/j.biortech.2005.08.001

[19] Arslan-Alaton I, Balcioglu IA, Bahnemann DW. Advanced oxidation of a reactive dyebath effluent: comparison of O3, H2O2/UV-C and TiO2/UV-A processes. Water Res. 2002; 36: 1143-54. https://doi.org/10.1016/S0043-1354(01)00335-9

[20] Bankian G, Mehrvar M. Integration of advanced oxidation technologies and biological processes: recent developments, trends and advances. J Environ Sci Health A. 2004; 39(11-12): 3029-81. https://doi.org/10.1081/LESA-200034939

[21] Ehssan MN. Utilization of bentonite as an adsorbent material in the removal of iron (III). Int J Eng Sci Technol. 2012; 4(10): 4480.

[22] Golob V, Vinder A, Simonic M. Efficiency of the coagulation/flocculation method for the treatment of dyebath effluents. Dyes Pigm. 2005; 67(2): 93-7. https://doi.org/10.1016/j.dyepig.2004.11.003

[23] Gutierrez MC, Pepió M, Crespi M. Electrochemical oxidation of reactive dyes: method validation and application. Color Technol. 2002; 118(1): 1-5. https://doi.org/10.1111/j.1478-4408.2002.tb00129.x

[24] Al-Degs YS, El-Barghouthi MI, El-Sheikh AH, Walker GM. Effect of solution pH, ionic strength, and temperature on adsorption behavior of reactive dyes on activated carbon. Dyes Pigm. 2008; 77(1): 16-23. https://doi.org/10.1016/j.dyepig.2007.03.001

[25] Arivoli S, Nandhakumar V, Saravanan S. Adsorption dynamics of copper ion by low-cost activated carbon. Arab J Sci Eng. 2009; 34(1A): 1-12.

[26] Ndive JN, Onukwuli OD, Obiora-Okafo IA. Exploring the characterization of Cactus opuntia as a coagulant for turbidity and chromium removal from simulated paint wastewater. Int Res J Adv Eng Sci. 2021; 6(3): 363-70.

[27] Muko-Okoro CE, Obiora-Okafo IA, Ndive JN. Investigation of the adsorption potentials of an organic adsorbent for phenol removal from aqueous solution. J Eng Res Rep. 2021; 20: 124-34. https://doi.org/10.9734/jerr/2021/v20i517318

[28] Kim S, Park C, Kim TH, Lee JW, Kim SW. COD reduction and decolorization of textile effluent using a combined process. J Biosci Bioeng. 2003; 95(1): 102-5. https://doi.org/10.1016/S1389-1723(03)80156-1

[29] Ndive JN, Obiora-Okafo IA, Onukwuli OD. Optimization studies on the coagulation-flocculation process for PWW treatment using Cactus opuntia extract: comparative studies for performance evaluation. J Basic Appl Res Int. 2023; 29(4): 16-31. https://doi.org/10.56557/jobari/2023/v29i48409

[30] Kim TH, Park C, Lee J, Shin EB, Kim S. Pilot scale treatment of textile wastewater by combined process (fluidized biofilm process–chemical coagulation–electrochemical oxidation). Water Res. 2002; 36(16): 3979-88.

[31] Rajeshkannan R, Rajasimman M. Sorption of Acid Blue 9 using Hydrilla verticillata biomass-optimization, equilibrium, and kinetics studies. Bioremediation J. 2011; 15(1): 57-67. https://doi.org/10.1080/10889868.2010.548002

[32] Hameed BH, Mahmoud DK, Ahmad AL. Equilibrium modeling and kinetic studies on the adsorption of basic dye by a low-cost adsorbent: coconut (Cocos nucifera) bunch waste. J Hazard Mater. 2008; 158(1): 65-72. https://doi.org/10.1016/j.jhazmat.2008.01.034

[33] Dotto GL, Moura JM, Cadaval TRS, Pinto LAA. Application of chitosan films for the removal of food dyes from aqueous solutions by adsorption. Chem Eng J. 2013; 214: 8-16. https://doi.org/10.1016/j.cej.2012.10.027

[34] Ahmad AA, Hameed BH, Aziz N. Adsorption of direct dye on palm ash: kinetic and equilibrium modelling. J Hazard Mater. 2007; 141(1): 70-6. https://doi.org/10.1016/j.jhazmat.2006.06.094

[35] Cooney EL, Booker NA, Shallcross DC. Ammonia removal from wastewaters using natural Australian zeolite. Sep Sci Technol. 1999; 34(12): 2307-27. https://doi.org/10.1081/SS-100100774

[36] Tilley SD, Schreier M, Nazeeruddin MK, Park NG. Water photolysis at 12.3% efficiency via perovskite photovoltaics and earth-abundant catalysts. Science. 2014; 345: 292-5. https://doi.org/10.1126/science.1258307

[37] Senthilnathan J, Philip L. Photocatalytic degradation of lindane under UV and visible light using N-doped TiO2. Chem Eng J. 2010; 161(1-2): 83-92. https://doi.org/10.1016/j.cej.2010.04.034

[38] Brown DH, Brown RM (1991) Mineral cycling and lichens: the physiological basis. Lichenologist. 2007; 23: 293–307. https://doi.org/10.1017/S0024282991000440

[39] Al Sagheer FA, Al-Sughayer MA, Muslim S, Elsabee MZ. Extraction and characterization of chitin and chitosan from marine sources in Arabian Gulf. Carbohydr Polym. 2009; 77(2): 410-9. https://doi.org/10.1016/j.carbpol.2009.01.032

[40] Yen MT, Yang JH, Mau JL. Physicochemical characterization of chitin and chitosan from crab shells. Carbohydr Polym. 2009; 75(1): 15-21. https://doi.org/10.1016/j.carbpol.2008.06.006

[41] Koyuncu I. Reactive dye removal in dye/salt mixtures by nanofiltration membranes containing vinylsulphone dyes: effects of feed concentration and cross flow velocity. Desalination. 2002; 143: 243-53. https://doi.org/10.1016/S0011-9164(02)00263-1

[42] Koch M, Yediler A, Lienert D, Insel G, Kettrup A. Ozonation of hydrolyzed azo dye reactive yellow 84 (CI). Chemosphere. 2002; 46: 109-113. https://doi.org/10.1016/S0045-6535(01)00102-3

[43] Yang X, Han F, Xu C, Jiang S, Huang L, Liu L, Xia Z. Effects of preparation methods on the morphology and properties of nanocellulose (NC) extracted from corn husk. Ind Crops Prod. 2017; 109: 241-7. https://doi.org/10.1016/j.indcrop.2017.08.032

[44] Malik PK. Dye removal from wastewater using activated carbon developed from sawdust: adsorption equilibrium and kinetics. J Hazard Mater B. 2004; 113: 81-8. https://doi.org/10.1016/j.jhazmat.2004.05.022

[45] Rajkumar D, Guk-Kim J. Oxidation of various reactive dyes with in situ electro-generated active chlorine for textile dyeing industry wastewater treatment. J Hazard Mater B. 2006; 136: 203-12. https://doi.org/10.1016/j.jhazmat.2005.11.096

[46] Mohan N, Balasubramanian N, Basha CA. Electrochemical oxidation of textile wastewater and its reuse. J Hazard Mater B. 2007; 147: 644-51. https://doi.org/10.1016/j.jhazmat.2007.01.063

[47] Torrades F, García-Montaño J, García-Hortal JA, Nuñez L, Doménech X, Peral J. Decolorisation and mineralisation of homo- and hetero-bireactive dyes under Fenton and photo-Fenton conditions. Color Technol. 2004; 120: 188-94. https://doi.org/10.1111/j.1478-4408.2004.tb00228.x

[48] Allegre C, Maisseu M, Charbit F, Moulin P. Coagulation-flocculation-decantation of dye house effluents: concentrated effluents. J Hazard Mater B. 2004; 116: 57-64. https://doi.org/10.1016/j.jhazmat.2004.07.005

[49] Jhawar M, Bartels C, Chilekar S. UF technology contributes to the recycling of dye salt solutions. Filtr Separat. 2003; 40: 20-1. https://doi.org/10.1016/S0015-1882(03)00031-4

Appendix

Table

Kinetic and Mechanistic Model	Parameter	BC	Fe_2O_3@BC-700
Pseudo first order model (PFO)	q_e pred. (mg/g)	49.70	99.67
	q_e exp. (mg/g)	61.90	88.75
	R^2	0.9755	0.9619
	k_f (min^{-1})	0.1059	0.1117
Pseudo second order model (PSO)	q_e pred. (mg/g)	63.694	92.592
	q_e exp. (mg/g)	61.90	88.75
	R^2	0.9988	0.9979
	k_s x 10^3 (g/mg min)	6.8852	3.3136
Elovich model	B	0.0772	0.0515
	α (mg/g min)	28.8265	33.1947
	R^2	0.8978	0.9421
Liquid film diffusion model	k_{fd} (min^{-1})	0.1044	0.1023
	R^2	0.9918	0.9505
Homogeneous solid film diffusion model	D_s (m^2/s)	0.1467	0.1635
	R^2	0.8165	0.8858
Weber-Morris	k_{ipd-1} (mg/g/$min^{1/2}$)	13.514	17.397
	q_{ipd-1} (mg/g)	2.817	2.8252
	R_1^2	0.9669	0.986
	k_{ipd-2} (mg/g/$min^{1/2}$)	2.4283	5.1971
	q_{ipd-2} (mg/g)	45.394	54.341
	R_2^2	0.8254	0.9327
	k_{ipd-3} (mg/g/$min^{1/2}$)	0.1571	0.654
	q_{ipd-3} (mg/g)	60.518	83.049
	R_3^2	0.8406	0.6657